Similarity of the crystal and solution structure of yeast tRNAPhe

Robillard, G.T.; Tarr, C.E.; Vosman, F.; Berendsen, H.J.C.

Published in:
Nature

DOI:
10.1038/262363a0

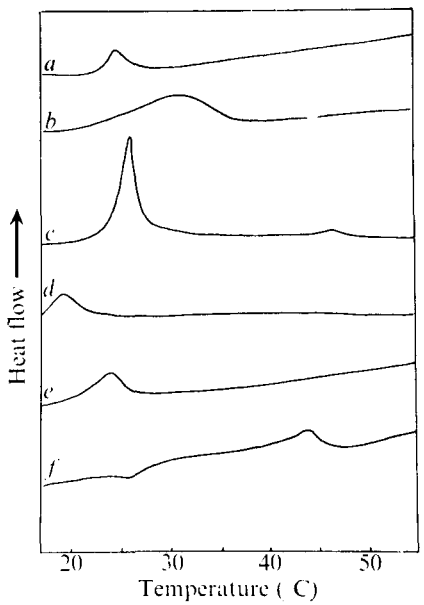

Fig. 3 Differential scanning calorimetry of DMPG vesicles in the presence of DMSO, dibucaine and calcium. *a*, Thermogram obtained from vesicles prepared in the presence of PBS alone. The remaining curves were obtained from vesicles to which were added: *b*, calcium chloride 5×10^{-4} M; *c*, DMSO 20% (v/v), 2.6 M; *d*, dibucaine hydrochloride 5×10^{-5} M; *e*, DMSO 20% (v/v), 2.6 M and dibucaine hydrochloride 5×10^{-5} M; *f*, DMSO 20% (v/v), 2.6 M, dibucaine hydrochloride 5×10^{-5} M, and calcium chloride 5×10^{-4} M. Dibucaine hydrochloride was obtained from K and D Laboratories, Plainview, New York.; calcium chloride from Upjohn Co., Kalamazoo, Michigan.

haem. Other manifestations of differentiation may therefore not be inhibited by the local anaesthetics.

Our studies suggest that the cryoprotective ability of these compounds may also be related to their membrane effects. It is possible that a decrease in fluidity of the cell membrane could render the cell and its subcellular organelles more resistant to distortion during freezing. In fact, preliminary experiments in our laboratory suggest that local anaesthetics may inhibit DMSO cryoprotection of erythrocytes.

Although not ruling out a direct effect on transcription, the studies reported here suggest that in FLC line 745A interaction of the cryoprotective inducers with the cell membrane may play an important part in the induction of differentiation of murine erythroleukaemic cells. A decrease in membrane fluidity could alter the transport and permeability properties of the membrane or cause the 'release' of an intracellular messenger which would itself be responsible for initiating the transcription of those mRNAs necessary for erythroid differentiation. On the other hand, the same physical interactions which occur between the agents and the phospholipid membranes and the associated water molecules could also occur at other sites within the cell (including proteins, or nucleic acids). The conformational changes produced at such sites[20,21] could result in differentiation by directly effecting the transcription of mRNAs associated with differentiation. Although these lipid vesicle studies seem to be predictive of the effects of cryoprotective agents on FLC line 745A, they are not predictive of their effects on line 745D, a cell line which is refractory to DMSO and only minimally responsive to other cryoprotective agents[2]. It thus seems possible that the difference in responsiveness between lines 745A and 745D may be a result of differences in their cell membranes.

We thank G. Christoff, E. Taylor, T. Isac and R. Lazo for technical assistance. This work was supported by US Public Health Service grants from the National Institutes of Health.

Received October 20, 1975; accepted May 25, 1976.

1 Preisler, H. D., and Lyman, G. H., *Cell Differentiation*, **4**, 179–815 (1975).
2 Preisler, H. D., Christoff, G., and Taylor, E., *Blood*, **47**, 363–368 (1976).
3 Preisler, H. D., Houseman, D., Scher, W., and Friend, C., *Proc. natn. Acad. Sci. U.S.A.*, **70**, 2956–2959 (1973).
4 Pollack, R. E., and Hough, P. V. C., *A. Rev. Med.*, **25**, 431–446 (1974).
5 Ladbrooke, B. D., and Chapman, D., *Chem. phys. Lipids*, **3**, 304–356 (1969).
6 Hinz, H. J., and Sturtevant, J. M., *J. biol. Chem.*, **247**, 6071–6075 (1972).
7 Linden, C. D., Wright, K. L., McConnell, H. M., and Fox, C. F., *Proc. natn. Acad. Sci. U.S.A.*, **70**, 2271–2275 (1973).
8 Overath, P., and Trauble, H., *Biochemistry*, **12**, 2625–2634 (1973).
9 Raison, J. K., *J. Bioenerg.*, **4**, 285–309 (1973).
10 Hubbell, W. L., Metcalfe, J. C., Metcalfe, S. M., and McConnell, H. M., *Biochim. biophys. Acta*, **219**, 415–427 (1970).
11 Papahadjopoulos, D.' Jacobson, K., Poste, G., and Shepard, G., *Biochim. biophys. Acta*, **394**, 504–519 (1975).
12 Papahadjopoulos, D., Jacobson, K., Nir, S., and Isac, T., *Biochim. biophys. Acta*, **311**, 330–348 (1973).
13 Bangham, A. D., Standish, M. M , and Watkins, J. C., *J. molec. Biol.*, **13**, 238–252 (1965).
14 Leder, A., and Leder, P., *Cell*, **5**, 319–322 (1975).
15 Rammler, D. H., and Zafferoni, A., *Ann. N. Y. Acad. Sci.*, **141**, 13–23 (1967).
16 Colley, C. M., and Metcalfe, J. C., *FEBS Lett.*, **24**, 241–246 (1972).
17 Jacobson, K., and Papahadjopoulos, D., *Biochemistry*, **14**, 152–161 (1975).
18 Trauble, H., and Eibl, H., *Proc. natn. Acad. Sci. U.S.A.*, **71**, 214–219 (1974).
19 Bernstein, A., Boyd, A. S., Brichley, V., and Lamb., V., in *Biogenisis and Turnover of Membrane Macromolecules* (edit. by Cook, J. S.), 145–159 (Raven, New York, 1976).
20 Henderson, T. R., Henderson, R. F., and Johnson, G. E., *Arch. Biochem. Biophys.*, **132**, 242–248 (1969).
21 Herskovits, T. T., *Archs Biochem. Biophys.*, **97**, 474–484 (1962).
22 Lyman, G.H., Papahadjopoulos, D., and Preisler, H.D., *Biochim. biophys. Acta* (in the press).

Similarity of the crystal and solution structure of yeast tRNA^{Phe}

G. T. Robillard, C. E. Tarr*, F. Vosman & H. J. C. Berendsen

Department of Physical Chemistry, University of Groningen, Zernikelaan, Groningen, The Netherlands

A comparison of the crystal and the solution structure of yeast tRNA^{Phe} has been carried out by calculating the low field NMR spectrum from refined X-ray structure coordinates. The similarity between the computed and observed spectra show that the crystal and solution structure are virtually identical.

* Permanent address: Department of Physics, University of Maine, Orono, Maine 04473.

NUCLEAR magnetic resonance (NMR), in theory, can provide information on the solution structure of a macromolecule at the same level of resolution as obtained with X rays in solids. In particular, the chemical shift and relaxation parameters contained in an NMR spectrum are sensitive functions of the local environments of individual nuclei. Nevertheless, the transition from the theoretical argument to the practical task of attempting to extract such information from NMR spectra poses significant problems since the magnitude of individual effects are not precisely known and difficult to calculate.

Table 1 Optimised ring current values

Nucleotide	Ring currents Giessner-Prettre and Pullman[6]	Optimised
Adenine		
Hexagonal ring	0.88	0.763
Pentagonal ring	0.67	0.580
Guanine		
Hexagonal ring	0.25	0.288
Pentagonal ring	0.63	0.725
Cytosine	0.27	0.210
Uracil	0.08	0.107

Calculation of magnetic ring currents, however, has reached a significantly high level of accuracy to be useful in predicting resonance positions if these positions, to a reasonable approximation, are determined only by ring current effects. In the case of NMR spectra of tRNA it is likely that ring currents are the dominant shift mechanism determining resonance positions.

Each ring NH · · · N hydrogen bonded proton in a Watson–Crick base pair generates a resonance in the low field region of the proton NMR spectrum of tRNA[1]. The chemical shift of a proton in such an environment is a combination of three principal effects: (1) deshielding by polarisation of the NH bond due to the adjacent electronegative atoms of the hydrogen bond; (2) deshielding arising from the ring currents of the two aromatic rings between which this hydrogen bonded proton is located; and (3) shifts caused by the ring currents of bases stacked above and below the base pair containing the proton in question. The magnitude of these three effects may be as large as several parts per million. All other shift mechanisms generate shifts on the order of a few tenths of a part per million.

Since the X-ray structure of yeast $tRNA^{Phe}$ has now been solved[2,3] and refined coordinates are available, we have calculated, directly from the coordinates, the ring current shift which each hydrogen bonded proton experiences from all other aromatic rings in the molecule. The results show that, on the basis of the resulting NMR spectrum, the X-ray crystal structure and the solution structure are virtually identical.

Fig. 1 360-MHz proton NMR spectra of yeast $tRNA^{Phe}$ in H_2O solutions taken at 35 °C. The spectra represent 1-h accumulations in the continuous wave mode with a sweep rate of 12 s per 2,400 Hz. Solvent composition was: *A*, 1 mM tRNA, 1 mM EDTA and 10 mM sodium cacodylate *p*H 7; *B*, 1 mM tRNA, 1 mM EDTA, 10 mM sodium cacodylate *p*H 7, 15 mM $MgCl_2$, 0.1 M NaCl.

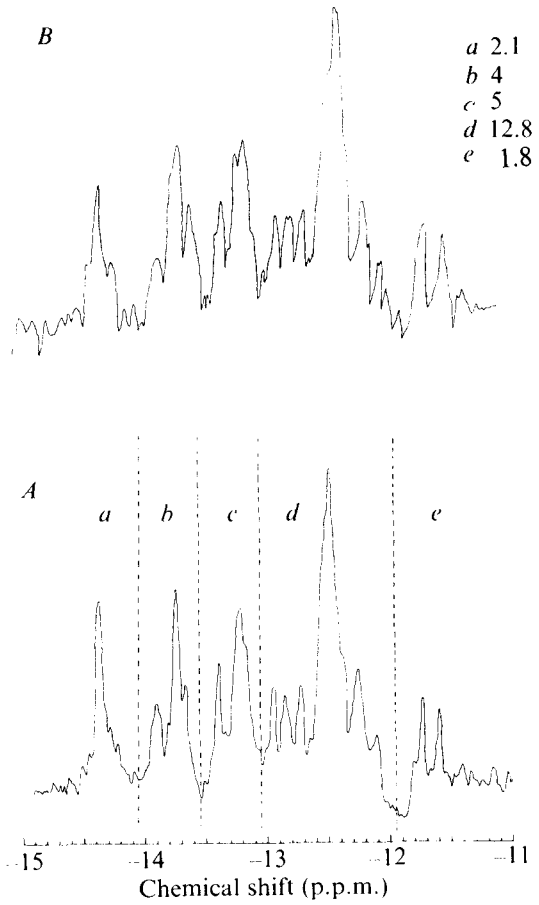

Ring current calculations

We have used the theory of Haigh and Mallion[4] to calculate the ring current shifts of the hydrogen bonded protons. In this theory, which is based on McWeeny's quantum mechanical treatment[5], all contributions to the ring current shifts are standard geometric terms that are calculated from the positions of ring atoms, multiplied by a factor proportional to the magnitude of the ring current. Haigh and Mallion used an empirical factor that is relevant only for in-plane protons attached to aromatic ring systems, but that should be scaled up by a factor of 2.6 for large distances. We have used this factor of 2.6 as appropriate for the distances occurring in tRNA. Our program for calculating the ring current shifts places a proton on a straight line between the donor and acceptor nitrogens at a distance of 1.02 Å from the donor. It then sums the ring current contributions of every ring in the molecule excluding the donor and acceptor rings for the base pair of interest. These rings are considered separately when determining starting positions for a hydrogen bonded proton in a given type of base pair.

Ring currents for the four isolated bases A, G, U and C have been calculated by Giessner-Prettre and Pullman[6] and are expressed relative to the ring currents in benzene (see Table 1). For several reasons calculated values of ring currents can be considered to be only approximately correct: (1) ring currents, derived from second-order perturbation theory, are sensitive to approximations used in the quantum mechanical treatment; (2) in hydrogen bonded base pairs the ring currents may deviate substantially from those in isolated bases; (3) the neglect of the effect of charges in heterocyclic rings; and (4) the inaccuracy of the geometric terms used in the calculation of shifts all may influence the apparent ring currents. Empirical adjustments for each of the ring currents should therefore be made to properly account for the observed shifts. We used the calculated ring currents[6] as starting values in an iterative procedure that successively refined each value. First, the A and G ring currents, and the difference between the AU and GC starting positions were varied and the computer was allowed to make a best fit between the nearest members of the calculated and the observed spectra. Then the C and U ring currents were refined keeping A and G fixed. These new values then provided the basis for a final slight refinement of A and G ring currents. In each case, the pentagonal and hexagonal ring currents of each purine were varied by the same factor, thus leaving only four ring currents to be refined. Because of the rapid convergence of this technique, no further iteration was required. A major advantage of this procedure is that one is not required to make detailed *a priori* assignments of given base pairs to specific resonances in the observed spectrum and thereby prejudice the outcome.

The values arrived at by this optimisation procedure are listed in Table 1. As can be seen, the optimum values for this calculation are only slightly different from the values calculated by Giessner-Prettre and Pullman[6]. Furthermore, the changes are consistent with those expected from hydrogen bonding between base pairs. During hydrogen bonding the electron density in the electron cloud, and hence the ring current, is expected to increase on the donor base and decrease on the acceptor base. This is precisely what occurs when the ring

Table 2 Base pair ring current shift

Helix	Base pair	Ring current shift (p.p.m.)
Acceptor	GC 1	+1.2244
	CG 2	+1.0705
	GC 3	+1.4032
	AU 5	+0.6150
	UA 6	+0.6151
	UA 7	+1.0451
DHU	GC 10	+0.9852
	CG 11	+0.4379
	UA 12	+0.3418
	CG 13	+0.5539
Anticodon	CG 27	+1.1602
	CG 28	+1.9580
	AU 29	+1.1530
	GC 30	+0.9366
	AΨ 31	+0.2392
TUC	CG 49	+1.3464
	UA 50	+1.5445
	GC 51	+1.2773
	UA 52	+1.1299
	GC 53	+0.9840
Tertiary	U8–A14	+0.5369
	T54–A58	+0.4942
	G22–m^7G46	+1.7710
	G19–C56	+0.8615
	m^2_2G26–A44	+0.4052
	G15–C48	+0.4003

currents are optimised. We are confident, therefore, that the optimisation procedure has not led to incorrect answers.

Yeast tRNA^{Phe} NMR spectrum

For the purpose of making detailed comparisons between observed and calculated spectra, it was necessary to use the most highly resolved spectra of tRNA^{Phe} available. Figure 1 shows the low field NMR spectra of yeast tRNA^{Phe} taken at 360 MHz in the absence or presence of Mg^{2+} (B. R. Reid, personal communication). Except for slight shifts in resonance positions and the narrowing of the resonances in the absence of Mg^{2+}, the two spectra are identical. Because of the higher magnetic fields and the special solvent conditions, however, the resolution in the no Mg^{2+} spectrum (Fig. 1*A*) reveals a number of features not observed in previously published spectra of this molecule[7–10]. There are seven well resolved resonances below −11.5 p.p.m. all of which have approximately unit intensity. When the total integrated intensity in the spectrum is calculated relative to any one of these individual resonances we find 26 ± 1 protons between −15 and −11.5 p.p.m. as shown in the table on the side of spectrum in Fig. 1*B* (B. R. Reid and G. T. R., in preparation). Similar spectral resolution plus an independent calibration on the high field methyl resonances has led us recently to the same conclusion in the case of *Escherichia coli* $tRNA_1^{Val}$ (refs 11 and 12). The intensity in the low field region of yeast tRNA^{Phe} must then be attributed to the 20 secondary structure Watson–Crick hyrodgen bonded base pair protons

Table 3 Proton resonance positions

Base pair	Chemical shift (p.p.m.) Calculated	Observed
UA 12	−14.01	−13.91
AU 5	−13.74	−13.72
UA 6	−13.74	−13.72
UA 7	−13.31	−13.38
UA 52	−13.22	−13.25
AU 29	−13.20	−13.22
AU 31	−13.18	−13.18
CG 11	−13.10	−13.16
CG 13	−12.98	−12.93
UA 50	−12.81	−12.83
GC 30	−12.60	−12.57
GC 10	−12.55	−12.51
GC 53	−12.55	−12.49
CG 2	−12.47	−12.47
CG 27	−12.38	−12.42
GC 1	−12.31	−12.39
GC 51	−12.26	−12.27
CG 49	−12.19	−12.23
GC 3	−12.13	−12.09
CG 28	−11.58	−11.58
T54–A58	−14.38	−14.40
U8–A14	−14.42	−14.40
G19–C56	−12.68	−12.72
G22–m^7G46	−12.47	−12.47
G15–C48	−11.78	−11.72
m^2_2G26–A44	−13.81	−13 81

Base pair offsets: Watson–Crick AU, −14 35; Watson–Crick GC, −13.54; reversed Hoogstein AU, −14.90; AΨ≃ −13.50.

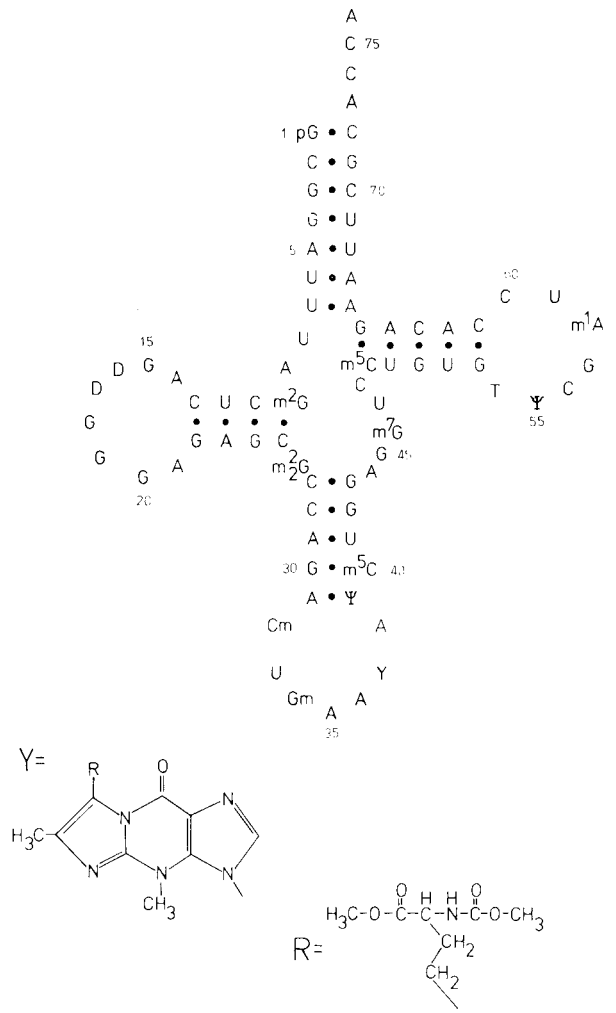

Fig. 2 Cloverleaf sequence of yeast tRNA^{Phe} (refs 14 and 15).

(Fig. 2) plus hydrogen bonded protons from tertiary interactions. There are five tertiary interactions involving ring NH· · ·N type hydrogen bonds which should account for five of the resonances in this region. Only one proton resonance is left unaccounted for and its origin will be discussed in the following section.

Figure 3*A* is a computer fit of the original spectrum in Fig. 1*A*. It was prepared by assigning a number of Lorentzian lines of equal intensity and linewidths to the positions where they occur in the original spectrum. Twenty-six lines were used to generate this spectrum and comparison with Fig. 1 demonstrates that the integration shown in this figure accurately reflects the number of protons in each peak of the original spectrum. The individual positions used in this fit were the same as those used in the ring current optimisation discussed above. The optimised ring current values for the four bases obtained by this procedure (Table 1) have been used in the Haigh and Mallion ring current

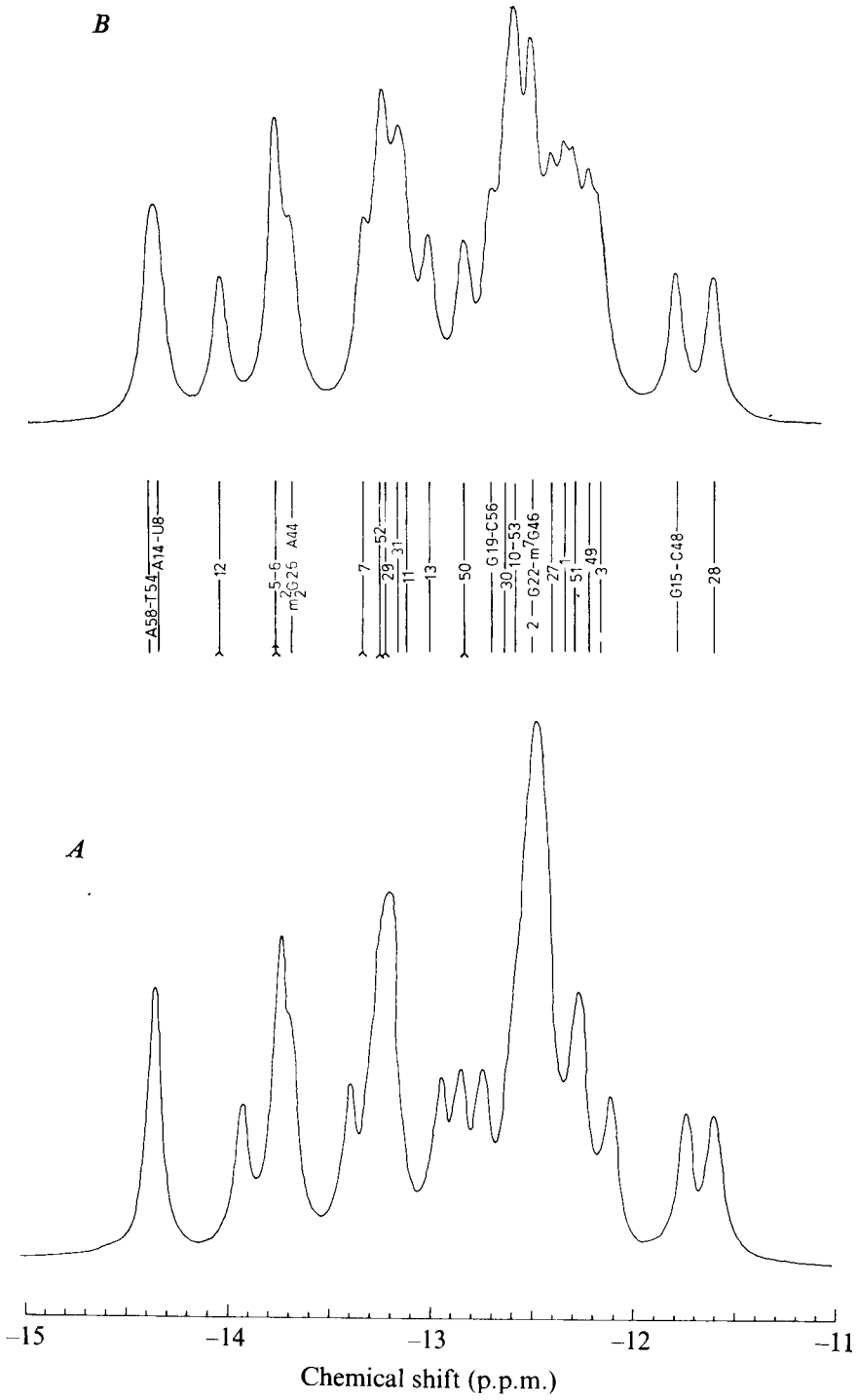

Fig. 3 *A*, Computer fit of the spectrum in Fig. 1*A* prepared as described in the text; *B*, spectrum calculated from the X-ray structure coordinate and optimised ring current values using the procedures and offsets described in the text and Tables 1–3. The indicated base pair positions are those assigned by the computer from the calculations. Secondary structure resonances are denoted by the normal conventions 1, 2 .... Secondary structure AU resonances are denoted by an ^ at the bottom of the line. Tertiary structure resonances are denoted by the full lettering and numbering of the base pair, that is, U8–A14 and so on.

calculation along with the X-ray crystal structure coordinates of yeast $tRNA^{Phe}$ refined by Sussman and Kim (personal communication). The resulting spectrum (Fig. 3*B*) compares very closely with the original (Fig. 3*A*). Since the NMR spectrum of $tRNA^{Phe}$ can be quite accurately calculated from the crystal structure coordinates simply by summation of the ring currents arising from each aromatic substituent in the molecule, there must be a very high degree of similarity between the solution and crystal structure.

Resonances from secondary structure base pairs

A base pair hydrogen bonded proton will experience deshielding ring currents from the aromatic rings of the donor and acceptor bases. If the distance between the donor and acceptor bases varies slightly, as they do in the refined crystal structure coordinates (2.8–3.1 Å), there will be slight alterations in the ring current shift. Since it is not clear, however, that these differences are physically meaningful at the current level of resolution of the X-ray coordinates, they have been ignored in the present calculations. Any error which results from this approximation will be small since the differences in degree of deshielding originating from these slight changes amount to only a few Hz. Deshielding also arises from the electronegative atoms of the hydrogen bond as stated previously. Since it is impossible to determine accurately the hydrogen bond strengths and correlate them with deshielding effects we have again assumed that the deshielding arising from the hydrogen bonded situation of the proton is the same for a given type of base pair. Thus the starting position for a proton in each type of isolated base pair is allowed to be a variable in the optimisation procedure discussed above. The parameters found were −14.35 and −13.54 p.p.m. for Watson–Crick AU and GC base-paired hydrogen bonded protons, respectively.

Resonance from Aψ base pair

The aromatic ring of the "Y" base is stacked in the anticodon loop, one ring removed from the Aψ base pair. In the present calculation the ring current shift arising from this base was calculated using the ring current value provided by B. Pullman (personal communication). The total ring current shift experienced by the Aψ hydrogen bonded proton is 0.24 p.p.m. In studies of the anticodon fragment of yeast $tRNA^{Phe}$, Lightfoot *et al.*[9] found the Aψ resonance occurring in region *c* of Fig. 2 and set the starting position at −13.5 p.p.m. We find that the Aψ could occur in either region *b* or *c* depending on the starting position and the magnitude of the ring current shift which the proton experiences. In the absence of other information, therefore, we prefer to rely tentatively on the fragment studies and assign the resonance to region *c* with the Aψ starting position in the region of −13.5 p.p.m.

Resonances from tertiary structure interactions

The calculated resonance positions marked in Fig. 3 show that the two protons in region *a*, and one each in regions *b*, *c*, *d* and *e* are not normal Watson–Crick AU or GC secondary structure resonances. Having assigned AΨ 31 to region *c* in the previous section, the tertiary interactions must generate resonances in the remaining regions. The tertiary structure interactions involving U8–A14 and T54–A58 are of the reversed Hoogstein type (see Fig. 4*b*). These two tertiaries experience approximately the same ring currents as do the hydrogen bonded protons of AU5, 6 and 12 (see Table 2). If the AU offset is the same for both Watson–Crick and reversed Hoogstein base pairs, five protons fall into region *b* and none into region *a* of Fig. 1. It is probable, however, that protons in the reversed Hoogstein arrangement have a starting position

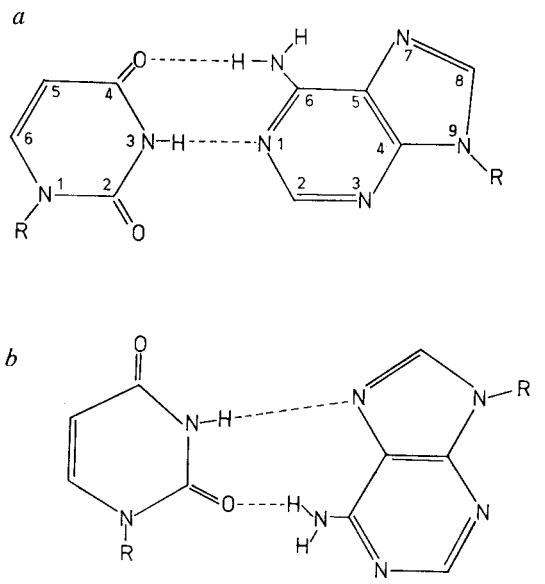

Fig. 4 Comparison of Watson–Crick AU base pairing (*a*) and reversed Hoogstein AU base pairing (*b*).

to lower field than Watson–Crick AU protons. In the reversed Hoogstein arrangement (Fig. 4*b*), the hydrogen bond acceptor is N7 of the five-membered ring instead of N1 of the six-membered ring. It has been shown by calculations on the tautomeric forms of purines[13] that the ring currents in both the hexagonal and pentagonal rings are a factor of 2–3 higher if a proton is attached to the N7 compared with the N1. The change in ring currents on hydrogen bonding N7 in place of N1 is

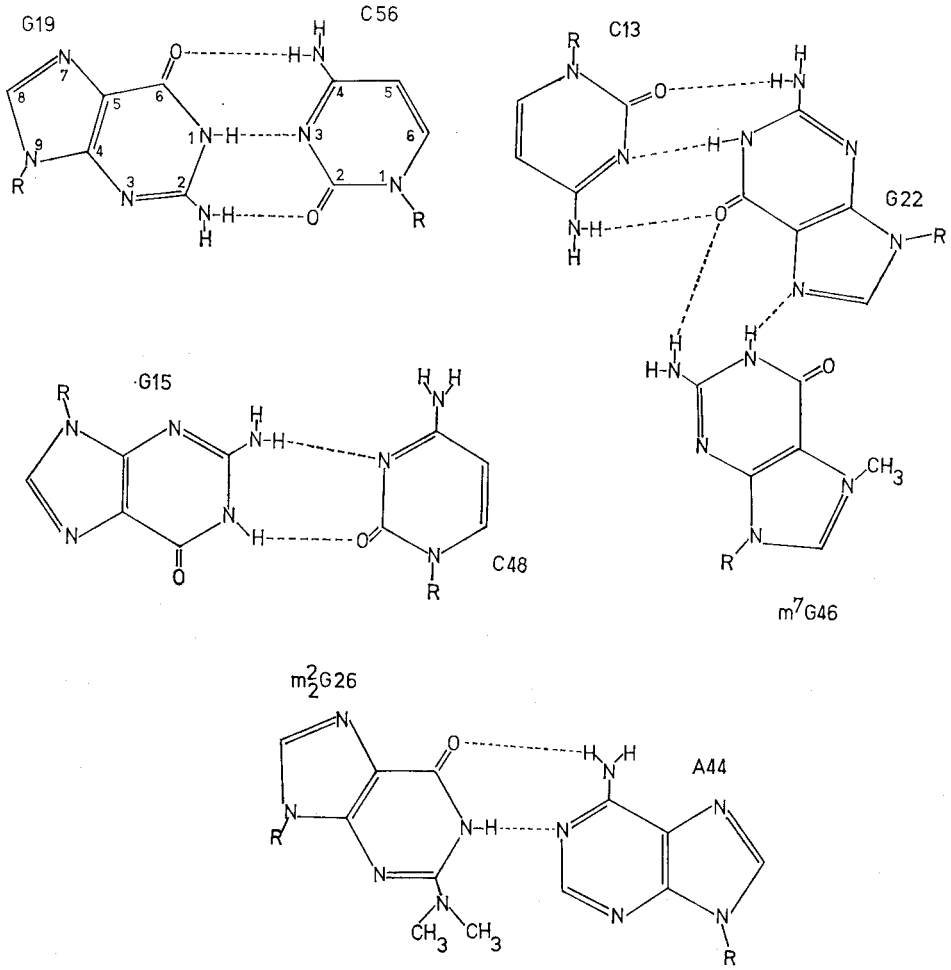

Fig. 5 Tertiary structure base pairing interactions, excluding the AU reversed Hoogstein, which are suggested to contribute resonances in the low field region of the NMR spectrum of yeast $tRNA^{Phe}$ (refs 2 and 3).

expected to be in the same direction. Thus the deshielding experienced by the proton in the reversed Hoogstein pair is expected to be greater than in the Watson–Crick base pair and the starting position should occur at lower field. Setting the reversed Hoogstein AU offset at −14.9 p.p.m. places the two tertiaries U8–A14 and T54–A58 in peak *a* at −14.4 p.p.m. A lower field starting position for the reversed Hoogstein base pair may also arise from a localisation of positive charge on the five-membered ring when hydrogen bonding occurs at N7. In contrast, the positive charge which develops when hydrogen bonding occurs at N1 in a Watson–Crick arrangement may be withdrawn from the ring by resonance interaction with the NH_2 group. A higher degree of positive charge on the ring would result in greater deshielding and a lower field position for the reversed Hoogstein AU base pair proton.

Figure 5 shows the remaining tertiary structure interactions which are likely to give rise to resonances in the −15 to −11.5 p.p.m. region of the NMR spectrum. Since G19–C56 is a normal Watson–Crick base pair we have used the standard GC starting position of −13.54 p.p.m. which places the resonance from this base pair in region *d* (see Fig. 3). Only one proton each in regions *b*, *d* and *e* remain unaccounted for. Allowing for the strong deshielding ring currents which should arise from both rings in the tertiary base pair m_2^2G26–A44, the starting position for this resonance should certainly be lower than a normal Watson–Crick GC and may be more nearly the same as a Watson–Crick AU proton resonance. Therefore, we have tentatively placed m_2^2G26–A44 in peak *b* with a starting position of −14.2 p.p.m. The G22–m⁷G46 interaction (Fig. 5), is of the reversed Hoogstein type. By analogy with the arguments presented for the AU reversed Hoogstein resonance starting positions we expect this GG reversed Hoogstein offset to be to lower field than a Watson–Crick GC starting position. The difference between a Watson–Crick and a reversed Hoogstein AU offset is 0.55 p.p.m. With the G22–m⁷G46 resonance assigned to region *d* at −12.47 p.p.m. the GG reversed Hoogstein interaction has a starting position of −14.2 p.p.m. (0.65 p.p.m. to lower field than the Watson–Crick GC interaction). The ring NH of G15 hydrogen bonded to the exocyclic oxygen of C48 should be less deshielded than a normal Watson–Crick GC and we have tentatively assigned this proton to region *e* as indicated in Fig. 3 with a low field starting position of approximately −12.1 p.p.m.

Comparison with previous NMR data

The original analysis of the yeast $tRNA^{Phe}$ NMR spectrum was made with considerable help from NMR spectra of fragments of the individual helices[9]. Since the helical region structure was expected to be fairly stable in the presence or absence of the rest of the molecule, the spectra obtained were assumed to reflect the resonance positions of the base pairs for a given helix in the intact molecule. If one compares the fragment data with the assignments which have evolved from the present calculations of the secondary structure resonance positions, it is immediately evident that the present assignments are in very close agreement with the fragment data. The only noticeable deviation is the assignment of GC 13 in the DHU helix which was originally assigned to one of the two highest field resonances. Our calculations show, however, that GC 13 suffers very little upfield shift (see Fig. 3 and Table 2).

The major change which must be made as a result of these studies is that the Watson–Crick AU starting position is changed to −14.35 p.p.m. In the early studies, without knowledge of AU tertiary structure resonances it was necessary to set the offset to lower field to account for the resonances which occurred below −14 p.p.m. This, however, necessitated raising the A and G ring currents 20% above published values.

The results of removing the sulphur from thiouridine in *E. coli* $tRNA_1^{Val}$ (ref. 11) provide further support for assigning the resonances in region *a* of Fig. 1, to the tertiary AU resonances. When the sulphur was removed from s_4U8 by cyanogen bromide treatment the resonance which occurred at −14.9 p.p.m. in the NRM spectrum of *E. coli* $tRNA_1^{Val}$ disappeared and was replaced by a new resonance at −14.2 p.p.m. This treatment should have changed a s_1U8–A14 tertiary base pair into a normal U8–A14 tertiary base pair as we have in yeast $tRNA^{Phe}$. The new resonance which appeared was located very close to that which we have assigned to the U8–A14 tertiary in the present spectra.

Kallenbach *et al.*[16] observed resonances at −13.8 and −13.2 p.p.m. when studying AMP interacting with oligo(U_{15}). Assuming the Watson–Crick AU offset of −14.6 p.p.m. originally used by Shulman *et al.*[8], the −13.8 p.p.m. resonance was assigned to ring NH · · · N Watson–Crick interactions while the −13.2 p.p.m. resonance was assigned to hydrogen bonded protons in the reversed Hoogstein interactions. The offsets proposed in this paper reverse the order of these assignments. Furthermore, when these offsets are used in conjunction with new ring current shift tables (Robillard *et al.*, in preparation) the position of the Watson–Crick and reversed Hoogstein resonance interactions for this polymer are predicted to occur exactly at the observed positions.

In their studies of ribosyl ApApGpCpUpUp double-stranded helix, Kan *et al.*[17] observed an AU resonance assigned to the internal AU base pair. At 0° the resonance occurred at −14.2 p.p.m. Since this base pair proton is expected to receive an upfield shift of approximately 0.5 p.p.m. from the neighbouring G, it would seem that the present starting position of −14.35 p.p.m. for a Watson–Crick AU base paired proton resonance is incorrect. It should be realised, however, that the temperature-dependent measurements of this fragment show a continuing shift as a function of decreasing temperature even after changes in the resonance line widths have ceased. As has been shown[17], this could arise from a structural change in the helix geometry (fraying effects). Thus it is likely that these fragments studies are not directly comparable with studies on larger polymers.

Conclusions

Table 3 contains the resonance positions of the protons in the observed spectrum and compares them with those which we have calculated using the offsets given at the bottom of the table and the ring current shifts in Table 2. The r.m.s. error between the resonances in the two columns is less than 0.05 p.p.m. (18 Hz) when only the 20 secondary structure resonances are included. The agreement between the calculated and observed positions, which is even within the observed linewidth, can be considered as very satisfactory since in the optimisation procedure only five adjustable parameters were used to calculate 20 relative line positions. These parameters were the four ring currents and the difference between the AU and GC starting positions. The deviations which are still observed may well represent slight differences between crystal and solution structure. They may also arise from a slightly incorrectly refined structure in one part of the molecule. Further experiments are in progress to examine these possibilities as well as the accuracy of our optimised ring currents and starting positions for the individual base pair types.

We thank the ZWO (Netherlands Foundation for Pure Research) for support of the high resolution NMR facility at the University of Groningen, B. Pullman for providing the "Y" base ring current, R. Kaptein for assistance with the ring current calculation programmes, and R. G. Shulman and B. R. Reid for their stimulating ideas and suggestions. We would also like to thank S. H. Kim for providing refined coordinates as soon as they were available.

Received April 28; accepted June 2, 1976.

1 Kearns, D. R., Patel, D., Shulman, R. G., and Yamane, T., *J. molec. Biol.*, **61**, 265–270 (1970).
2 Quigley, G. J., *et al.*, *Proc. natn. Acad. Sci. U.S.A.*, **72**, 4866–4870 (1975).
3 Ladner, J. E., *et al.*, *Proc. natn. Acad. Sci. U.S.A.*, **72**, 4414–4418 (1975).
4 Haigh, C. W., and Mallion, R. B., *Molec. Phys.*, **22**, 955–970 (1971).
5 McWeeny, R., *Molec. Phys.*, **1**, 311–321 (1958).

6 Giessner-Prettre, C., and Pullman, B., *C.r. hebd. Séanc. Acad. Sci., Paris*, **261**, 2521–2523 (1965).
7 Wong, Y. P., Kearns, D. R., Reid, B. R., and Shulman, R. G., *J. molec. Biol.*, **72**, 725–740 (1972).
8 Shulman, R. G., Hilbers, C. W., Kearns, D. R., Reid, B. R., and Wong, Y. P., *J. molec. Biol.*, **78**, 57–69 (1973).
9 Lightfoot, D. R., Wong, K. L., Kearns, D. R., Reid, B. R., and Shulman, R. G., *J. molec. Biol.*, **78**, 71–89 (1973).
10 Hilbers, C. W., Shulman, R. G., and Kim, S. H., *Biochem. biophys. Res. Commun.*, **55**, 953–960 (1973).
11 Reid, B. R., *et al.*, *Proc. natn. Acad. Sci. U.S.A.*, **72**, 2049–2053 (1975).
12 Reid, B. R., and Robillard, G. T., *Nature*, **257**, 287–291 (1975).
13 Giessner-Prettre, C., and Pullman, B., *C. r. hebd Séanc. Acad. Sci., Paris*, **268**, 1115–1117 (1969).
14 RajBhandary, U. U., *et al.*, *Proc. natn. Acad. Sci. U.S.A.*, **57**, 751 (1967).
15 Nakanishi, K., Furutachi, N., Funamizu, M., Grunberger, D., and Weinstein, I. B., *J. Am. chem. Soc.*, **92**, 7617 (1970).
16 Kallenbach, N. R., Daniel, W. E., and Kaminker, M. A., *Biochemistry*, **15**, 1218–1224 (1976).
17 Kan, A. S., Borer, P. N., and Ts'o, P. O. P., *Biochemistry*, **14**, 4864–4869 (1975).

letters to nature

The 21-cm absorption line in NGC1275

DE YOUNG, Roberts and Saslaw[1] detected H I absorption in NGC1275 with a velocity of 8,120 km s^{-1}. This is ~ 3,000 km s^{-1} larger than the systemic velocity of NGC1275 and is the same as that of the enigmatic system of gas filaments extending 40″ from the nucleus[2,3]. The observations of De Young *et al.* were made with a single dish with insufficient angular resolution to determine which of the various radio continuum sources were being absorbed. They argue that the absorption is probably occurring in the components < 0.2″ rather than in the 5′ halo component, but they were unaware of an intermediate scale 30″ component[4]. Here we present observations made with sufficient angular resolution to decide unambiguously between these possibilities. Our data can also be used to place a limit on the H I mass of possible foreground objects which could be causing the absorption.

Table 1 Flux densities in each channel

$c\Delta\lambda/\lambda_0$* (km s^{-1})	Average flux densities† (Jy) 'short' (50″)	'long' (20″)	Relative flux densities‡ (Jy) 'short' (50″)	'long' (20″)
8,085	10.86	9.37	−0.039	−0.053
8,126	10.62	9.14	−0.285	−0.291
8,167	10.89	9.41	−0.013	−0.017
8,209	10.91	9.42	−0.016	−0.008
8,250	10.91	9.42	−0.004	−0.006
8,291	10.91	9.43	0.005	0.001
8,332	10.92	9.43	0.011	0.004
8,373	10.90	9.43	−0.011	0.001

* Corrected to heliocentric.
† Calibrated with respect to 3C48 and 3C147 (assumed flux densities 15.91 and 21.90 respectively). The errors in these values are ±(0.007+1%).
‡ With respect to the channels with the highest four velocities.

The observations were obtained with the Westerbork Synthesis Radio Telescope and its 80-channel filter spectrometer[5]. The measurements with the ten shorter baselines (36–684 m in 72-m increments) were made on August 11, 1974, and those with the 10 longer baselines (756–1,404 m in 72-m increments) on November 15, 1974. The eight frequency channels have a half-power bandwidth of 129 kHz ($c\,\Delta\lambda/\lambda_0$ = 27 km s^{-1}) and cover the range in $c\Delta\lambda/\lambda_0$ from 8,085 to 8,373 km s^{-1}. Table 1 gives the amplitudes in each channel averaged at the position of the continuum source. For the shorter baselines this corresponds to the flux density from a region ~ 50″×75″ in diameter (EW×NS) centred on the nucleus of NGC1275. For the longer baselines this is the flux density from components < (20″×30″) at the position of the nucleus.

For each observation, the variations in amplitude for the highest four velocities are consistent with that expected from receiver noise, so we have taken the average of these four channels to represent the mean continuum amplitude and have also tabulated the amplitudes relative to this value. To compare our result with that of De Young *et al.*[1], we have convolved their profile with our broader bandpass, and we have used the more accurate gain calibration of the 300′ antenna[6]. This gives an absorption of 0.26±0.02 Jy, in agreement with our value of 0.287±0.006 Jy in the 8,085 km s^{-1} channel.

Table 2 lists the angular sizes and flux densities of the main components of NGC1275 at the epoch of these observations. The deepest absorption seen by De Young *et al.*[1] corresponds to 1.4 Jy, so it is possible that this could have occurred in any of the three continuum components. Figure 1*a* shows the fringe amplitude of continuum emission in position angles 0° and 90°. The three angular size scales as described by Miley and Perola[4] are clearly seen. In Fig. 1*b* we show the difference between the channel containing the strongest absorption and the channels containing the continuum. It is clear from this plot that the absorbed component is unresolved and we can place a limit of < 6″ EW and < 9″ NS on its angular size. Furthermore, from the interferometer phase we can see that the position of the absorbed component is within 1″ of the position of the small diameter continuum source.

From this we can exclude the possibility that the major part of the absorption is occurring in either the 3′×4′ halo component or the 30″ intermediate component but it is still possible

Fig. 1 *a*, The fringe amplitude of the continuum emission from NGC1275 in position angles 0° (×) and 90° (●) plotted against the interferometer baseline in wavelengths. Note that the amplitude scale is offset from zero. *b*, The difference between the channel containing the strongest absorption and the average of the channels containing the continuum emission.